# Two-Dimensional Deforming Finite Element Methods for Surface Ablation

M. Hogge* and P. Gerrekens†
*University of Liège, Liège, Belgium*

**This paper discusses the application of novel deforming finite element techniques to two-dimensional problems with moving boundaries caused by ablation. It is shown that deforming-grid techniques imply the construction of an additional convective matrix acting on the temperature unknowns. Surface ablation is taken into account by special boundary thermal loads. The usual finite elements are thus easily transformed for deforming grid purposes and allow for a precise tracking of the steep thermal gradients and localization of the surface. The numerical difficulties experienced in the procedure are discussed and solved. Illustration of the technique is made on model one- and two-dimensional axisymmetrical problems with carbonaceous and insulating materials.**

## Nomenclature

$c$ = heat capacity of the material per unit mass
$f_c$ = chemical ablation rate function
$f_m$ = mechanical ablation rate function
$g$ = total ablation function
$g_c, g_c^*$ = chemical ablation functions
$g_f, g_f^*$ = phase change ablation functions
$g_m$ = mechanical ablation function
$h$ = convection exchange coefficient
$H$ = boundary enthalpy
$H_a$ = fluid enthalpy
$H_c$ = specific heat per unit mass for chemical ablation
$H_m$ = specific heat per unit mass for mechanical ablation
$k$ = magnification factor for penetration depth
$L_f$ = specific latent heat per unit mass for phase change
$M$ = number of surface unknowns
$\mathfrak{M}$ = number of master lines
$n_i$ = direction cosines of the outward normal
$N$ = total number of unknowns
$\mathfrak{N}$ = number of unknowns along a master line
$p_e$ = external pressure at the boundary
$q_e$ = prescribed heat flux at the boundary
$q_\ell$ = nodal temperature unknowns
$r_i$ = residual vector
$\dot{s}$ = boundary normal velocity
$\dot{s}_c$ = boundary velocity due to chemical ablation
$\dot{s}_f$ = boundary velocity due to phase change
$\dot{s}_m$ = boundary velocity due to mechanical ablation
$S$ = boundary of the domain
$t$ = time variable
$T$ = local temperature within the material
$T_a$ = convection source temperature
$T_e$ = prescribed boundary temperature
$T_f$ = phase change temperature
$T_0$ = initial condition for temperature
$T_r$ = radiation source temperature
$u_i$ = grid nodal velocities
$v_\ell^c$ = nodal values of the chemical ablation velocity
$v_\ell^f$ = nodal values of the phase change velocity
$v_\ell^m$ = nodal values of the mechanical ablation velocity
$V$ = volume occupied by the domain
$x_i$ = Cartesian coordinate with respect to a fixed reference
$\alpha$ = convection exchange coefficient for enthalpy formulation
$\beta_w$ = boundary diffusivity
$\delta$ = one-dimensional heat penetration depth
$\epsilon$ = emissivity of the surface
$\eta$ = reduction coefficient for convective flux
$\lambda_{ij}$ = material thermal conductibility coefficients
$\rho$ = material density
$\sigma$ = Stefan-Boltzmann constant
$\tau$ = aerodynamic shear stress
$\psi_\ell$ = finite element shape functions

## Introduction

THIS paper deals with finite element techniques applied to the phase change and surface recession occurring in the thermal ablation of protective materials used on re-entry vehicles. Preliminary pyrolysis[1] of the material is not considered here.

Contrary to the cases of Stefan phase change problems,[2] it is assumed in ablation problems that the produced phase is removed instantaneously (at least in the scope of the present study) and that the domain of interest is thus continuously changing its shape. Such a global moving boundary implies the idea of deforming spatial grids in the context of the finite element method, even if fixed-grid solutions have also been presented.[3]

Numerical difficulties encountered in such discretizations can be cumbersome due to the moving-grid strategy and the (possible) low-conducting properties of the ablative material. In particular, steep gradients in the vicinity of the attacked boundary range in the magnitude of several hundred degrees per millimeter. Such sharp variations of the temperature field require an appropriate modeling technique to encompass the moving character of the grid.

The paper discusses first the field equations and boundary conditions outlining the temperature field of the ablative material and the surface ablation models that will be dealt with in the analysis.

The classical finite element equations are then transformed to take into account the continuous deformation of the grid. The price to pay is the construction of a corresponding convective matrix. The surface ablation equations are treated simultaneously with boundary velocity shape functions identical to the temperature ones.

Presented as Paper 83-1555 at the AIAA 18th Thermophysics Conference, Montreal, Canada, June 1-3, 1983; received Aug. 3, 1983; revision received May 4, 1984. 

*Senior Assistant, Aerospace Laboratory. Member AIAA.
†IRSIA Research Engineer, Aerospace Laboratory.

With the surface ablation equations making use of the thermal balance at the boundary, correct prediction of the surface velocity and position will depend greatly on the accurate modeling of the internal gradients near the boundary. It is demonstrated how a fine mesh within a zone of magnitude comparable with the so-called one-dimensional heat penetration depth[4] provides a suitable and extremely accurate answer to this problem. Explicit magnitudes of the penetration depths are given for various boundary condition types and histories.

The implementation of the deforming-grid technique in two dimensions is then described. All nodes of the finite element mesh are associated with a series of discretization lines linking the attacked surface to the internal surfaces. Each of these master lines will be deformed independently, as in a one-dimensional problem according to the magnitude of the local penetration depth along the line and to its surface node recession. The resulting transverse discretization lines are then deformed automatically.

We stress some of the numerical difficulties encountered in the solution procedure. These problems are linked with the permissible mesh velocity magnitude and the highly nonlinear character of the chemical ablation function.

Illustrations of the deforming grid techniques are given on model one- and two-dimensional situations with carbonaceous (high-ablation) and insulating (low-ablation) materials. They demonstrate the feasibility of the present modeling technique and its flexibility with respect to fixed-grid formulations.

## Field Equations and Boundary Conditions

The mathematical model of transient heat conduction including surface ablation is based on the heat equation,

$$(\lambda_{ij} T_{,j})_{,i} = \rho c \dot{T} \text{ in } V(t) \tag{1}$$

where the subscripts refer to components in the Cartesian axes ($i,j = 1, 2, 3$), a comma denotes the partial differentiation with respect to the space variables, and a superscript dot the time partial differentiation.

Appropriate boundary conditions are

$$T = T_e \qquad \text{on } S_1 \tag{2}$$

$$q_e + h(T_a - T) + \alpha(H_a - H) + \sigma\epsilon(T_r^4 - T^4) - n_i \lambda_{ij} T_{,j} = g \qquad \text{on } S_2(t) \tag{3}$$

The mathematical statement of the problem is completed by the initial condition

$$T(x_i, 0) = T_0(x_i) \text{ in } V_0 \tag{4}$$

The function $g$ appearing in Eq. (3) either depends on the ablation rate or vanishes according to the presence or lack of ablation. It will be called the ablation function.

## Surface Ablation Models

Two models of surface ablation are included in the analysis: 1) a Stefan (phase change) model with implicit knowledge of the surface movement that results directly from the thermal balance at the boundary and 2) an explicit model with full knowledge of this movement (by experimental data on chemical and mechanical ablation). Both models are based on the hypothesis that isotropic phenomena are confined at the boundary of the material.

### Stefan Model

In this model, the ablation function $g$ reads

$$g_f = \rho L_f \dot{s}_f \tag{5}$$

with

$$\dot{s}_f = 0 \text{ for } T < T_f, \quad \dot{s}_f \geq 0 \text{ when } T = T_f \tag{6}$$

In other words, when the surface temperature reaches the value $T_f$, ablation due to phase change (melting, sublimation, etc.) begins at a rate depending on the difference between the heat input and the net conduction flux penetrating the material [see Eq. (3)].

### Explicit Model

In this model, the ablation function $g$ is written

$$g_c = \rho H_c \dot{s}_c \tag{7}$$

where the surface recession due to chemical ablation

$$\dot{s}_c = f_c(t, T, p_e) \tag{8}$$

is a known function of time, surface temperature, and external pressure. Mechanical ablation (erosion) is also present in the model, i.e.,

$$\dot{s}_m = f_m(T, p_e, \tau) \tag{9}$$

which is a known function of surface temperature, external pressure, and aerodynamic shearing stresses, but does not contribute to the function $g$ since $H_m$ is usually negligible.

In this model, recession of the surface is known explicitely (but not directly) and yields the net conduction flux entering the material via the surface heat balance [see Eq. (3)].

### Combined and Modified Models

Both types of models may be present on part $S_2$ of the boundary. Thus, the total recession rate of the surface normal to the boundary reads

$$\dot{s} = \dot{s}_f + \dot{s}_c + \dot{s}_m \tag{10}$$

even if the two models usually govern distinct parts of $S_2$.

Let us finally note that the contributions of Eqs. (5) and (7) to the ablation function can be corrected to take into account the reduction of heat input due to the injection of ablation products into the thermal layer, i.e.,

$$g = g_f + g_c + \rho\eta(\dot{s}_f + \dot{s}_c)(H_a - H) = g_f^* + g_c^* \tag{11}$$

where $\eta$ is the appropriate reduction coefficient and, accordingly, $g_f^*$ and $g_c^*$ are modified ablation functions.

## Deforming Finite Element Formulation

### Heat-Transfer Equations

We stressed in the introduction the fact that the physics of the ablation phenomenon implies a variable domain and that it is thus natural to think of a discretization in terms of deforming finite elements. The spatial shape functions in the Galerkin weak form of the equations will then exhibit time dependency at a given location $x_i$ and we shall have

$$T(x_i, t) = \psi_\ell(x_i, t) q_\ell(t) \qquad (\ell = 1, 2, \ldots, N) \tag{12}$$

where the $q_\ell$ are the $N$ local values of the instantaneous temperature field acting as generalized coordinates of the problem.

The time derivative of the temperature is accordingly discretized as

$$\dot{T} = \psi_\ell \dot{q}_\ell + \dot{\psi}_\ell q_\ell \tag{13}$$

and implies, contrary to conventional fixed-grid formulations, the time rate of change for the shape functions. By

requiring that the shape functions themselves remain invariant at a given moving point, we can write equivalently[5]

$$\dot{T}=\psi_\ell \dot{q}_\ell - u_k \psi_{\ell,k} q_\ell \tag{14}$$

where $u_k$ $(k=1,2,3)$ denotes the grid deformation velocity at that point with respect to a fixed reference. The last term in Eq. (14) can thus be viewed as a transport term accounting for the convective effect of the grid motion.

Standard weighted residual-Galerkin treatment of the equations over the domain $V$ then leads to the weak form of the heat equation under the form of a system of semidiscretized differential equations in terms of nodal temperatures, collected in the global vector $\boldsymbol{q}$,

$$(\boldsymbol{K}-\boldsymbol{K}^d)\boldsymbol{q}+\boldsymbol{C}\dot{\boldsymbol{q}}=\boldsymbol{g}-\boldsymbol{g}^a \tag{15}$$

where $\boldsymbol{K}$, $\boldsymbol{C}$ and $\boldsymbol{g}$ are the conventional thermal conductivity matrix (internal and boundary contributions), the heat capacitance matrix, and the thermal load vector, respectively, with typical components of the form

$$K_{mn}=\int_{V(t)} \lambda_{ij}\psi_{m,i}\psi_{n,j}\,\mathrm{d}V+\int_{S_2}(h+h^*)\psi_m\psi_n\,\mathrm{d}S \tag{16}$$

$$C_{mn}=\int_{V(t)} \rho c\psi_m\psi_n\,\mathrm{d}V \tag{17}$$

$$g_m=\int_{S_2(t)}(q_e+hT_a+h^*T_r)\psi_m\,\mathrm{d}S \tag{18}$$

where

$$h^*=\sigma\epsilon(T_r^2+T^2)(T_r+T) \tag{19}$$

Thermal loads typical of the surface ablation phenomenon are gathered in the vector $\boldsymbol{g}^a$ directly built from the ablation rate function [Eq. (11)], written in terms of ablation velocities as

$$g_m^a=\int_{S_2(t)} g\psi_m\,\mathrm{d}S \tag{20}$$

The matrix $\boldsymbol{K}^d$ is the convective matrix accounting for the grid deformation and exhibits unsymmetrical components of the type

$$K_{mn}^d=\int_{V(t)} \rho c u_k \psi_{n,k}\psi_m\,\mathrm{d}V \tag{21}$$

All of these characteristic matrices depend, at least implicitely, upon time, the unknowns $q_n$ via $h^*$, and the eventual temperature dependence of $\lambda_{ij}$, $h$, $\rho c$, $q_e$, and $g$. Conventional nonablative fixed-grid formulations are simply restored by omitting Eqs. (20) and (21), i.e., by discarding $u_k$ and $g$ in the heat-transfer equations.

#### Surface Ablation Equations

The treatment of the internal heat and surface balances must be solved simultaneously to yield the ablation function required by Eq. (20).

Ablation velocities are interpolated with the same spatial shape functions as the temperature, leading to the following discretizations:

$$\dot{s}_f=\psi_\ell(x_i,t)v_\ell^f(t) \tag{22a}$$

$$\dot{s}_c=\psi_\ell(x_i,t)v_\ell^c(t) \tag{22b}$$

$$\dot{s}_m=\psi_\ell(x_i,t)v_\ell^m(t) \quad (\ell=1,2,\ldots,M) \tag{22c}$$

Note that the size of the discretizations is this time limited to the $M(\ll N)$ surface unknowns.

Weak forms of the ablation equations are then readily obtained via a Galerkin treatment limited to the part $S_2$ of the boundary subject to ablation,

$$\boldsymbol{L}^f\boldsymbol{v}^f=\boldsymbol{g}^f \tag{23a}$$

$$\boldsymbol{H}^c\boldsymbol{v}^c=\boldsymbol{g}^c \tag{23b}$$

$$\boldsymbol{H}^m\boldsymbol{v}^m=\boldsymbol{g}^m \tag{23c}$$

The particular components of the matrices and vectors appearing in these $(M\times M)$ systems are

$$L_{\ell n}^f=\int_{S_2(t)}\rho[L_f+\eta(H_a-H)]\psi_\ell\psi_n\,\mathrm{d}S \tag{24a}$$

$$H_{\ell n}^c=\int_{S_2(t)}\rho[H_c+\eta(H_a-H)]\psi_\ell\psi_n\,\mathrm{d}S \tag{24b}$$

$$H_{\ell n}^m=\int_{S_2(t)}\psi_\ell\psi_n\,\mathrm{d}S \tag{24c}$$

and

$$g_\ell^f=\int_{S_2(t)}(g-g_c^*)\psi_\ell\,\mathrm{d}S \tag{25a}$$

$$g_\ell^c=\int_{S_2(t)}\rho[H_c+\eta(H_a-H)]f_c\psi_\ell\,\mathrm{d}S \tag{25b}$$

$$g_\ell^m=\int_{S_2(t)}f_m\psi_\ell\,\mathrm{d}S \tag{25c}$$

where the total ablation rate function $g$ appearing in Eq. (25a) is written in terms of temperature and heat inputs via Eq. (3).

Let us recall that Eq. (23a) is subject to the constraints

$$v_\ell^f=0 \text{ if } q_\ell<T_f, \quad v_\ell^f\geq 0 \text{ if } q_\ell=T_f \tag{26}$$

## Steep Gradient Modeling

It stems from Eq. (3) that the correct prediction of the surface velocity will very much depend on the ability of the deforming-grid technique to represent accurately the internal gradients near the boundary. In common re-entry situations, these can range by magnitude of several hundred degrees per millimeter. Such sharp fronts in the temperature distribution must be dealt with by the deforming-grid technique. We shall briefly recall how a fine mesh in the vicinity of the boundary within a zone of magnitude comparable to the so-called one-dimensional penetration depth (PD) allows for a suitable and extremely accurate answer to this problem.[4]

#### Heat Penetration Depth Concepts

Although parabolic partial differential equations such as Eq. (1) behave as if infinite wave propagation speeds were implied, i.e., the influence of any perturbation at one point is felt instantaneously by any other point of the domain, one can decide on a threshold under which the temperature may be considered invariant during a certain period of observation, in keeping with the physical observance of finite penetration times of the heat inwards of the isothermal media.

The distance from the boundary beyond which the temperature within the domain is unaffected in one-dimensional situations is precisely the so-called penetration depth (PD).[6] There are other mathematical definitions of the PD—a convenient concept is the relative PD magnitude[7] based on the assumed spatial enthalpy distribution and governed by the

differential equation, which is, in the case of a semi-infinite medium exposed to $q_e(t)$ with surface velocity $\dot{s}(t)$

$$\frac{\mathrm{d}}{\mathrm{d}t}\left[q_e\frac{\delta^2}{\beta_w}\right]=q_e-\dot{s}\delta\frac{q_e}{\beta_w},\quad \delta(0)=0 \tag{27}$$

where $\beta_w$ is the boundary diffusivity $\lambda_{ij}n_in_j/\rho c$.

In the case of fixed boundary, a closed-form solution for Eq. (27) is

$$\delta(t)=\left[\frac{\beta_w(t)}{q_e(t)}\int_0^t q_e(\tau)\mathrm{d}\tau\right]^{1/2} \tag{28}$$

which depends on the instantaneous boundary diffusivity only and not on its history or internal variation. Particular heat inputs yield, for instance,

$$\delta_s(t)=[\beta_w t]^{1/2} \tag{29}$$

if $q_e(t)$ is a step function $q_e(t)=q_e\cdot u(t)$, where $u(t)$ denotes the Heaviside function and

$$\delta_r(t)=[\beta_w t/2]^{1/2} \tag{30}$$

if $q_e(t)$ is a ramp function $q_e(t)=q_e\cdot t$.

Combinations of heat inputs and other types of boundary conditions can be treated as well.[4] An interesting conclusion is that the PD magnitudes depend mainly on the shape of the boundary condition (not on its amplitude) and that the Dirichlet conditions exhibit larger PDs than heat input conditions.

#### Deforming Grid Strategy Based on PD Magnitude

Time-dependent PD magnitudes resulting from Eq. (27) yield the desired grid deformation law for the purposes of steep-gradient modeling in one dimension. Thus include $N_{PD}$ elements of the initial (uniform or nonuniform) grid in a zone $\delta_k(t)$ corresponding to $k$ times the instantaneous PD and dilate this zone as time proceeds according to

$$\delta_k(t)=k\cdot\delta(t) \tag{31}$$

where $k$ is an appropriate number that accounts for the boundary condition types and shapes. The corresponding $N_{PD}$ elements are consequently dilated and the remaining ones contracted. In all cases where $\beta_w$ and $\dot{s}$ are temperature independent, Eq. (27) and (28) yields an explicit function of time; otherwise, $\delta_k(t)$ is dependent upon the surface temperature and will vary during the iterative solution procedure. As a rule, the actual PD should in fact never underestimate the effective one. Numerical experiments have demonstrated that appropriate values of $k$ range in the interval 2-4 for most of the cases.[4]

## Two-Dimensional Deforming Grid Implementation

Grid deformations are thus developed with a double objective:

1) Track the moving boundary due to ablation and insure the corresponding contraction of the element sizes within the discretized domain.

2) Enable accurate modeling of the thermal gradients (especially if they are steep) in the vicinity of the moving boundary.

This is accomplished by separating the boundaries of the domain into three classes (see Fig. 1) as follows:

1) Attacked boundaries subject to ablation $S_A$ for which the node propagation will be normal to the surface.

2) Nonablative boundaries $S_{NA}$ for which all of the nodes remain fixed. If the whole boundary of the domain suffers ablation, an internal boundary is designated to play this role.

3) Special boundaries $S_S$ that are not directly subject to ablation, but adjacent to an ablative boundary and for which the corresponding direction of ablation is prescribed (e.g., the axis of symmetry).

All nodes of the finite element mesh are associated with discretization lines linking the attacked boundaries to the nonablative ones. These master lines do not necessarily coincide with the interelement boundaries, but they do not intersect within the moving grid domain. The whole grid exhibits $\mathfrak{M}$ of these lines. For each of them, we define a total number of nodes (say $\mathfrak{N}$) and, if the grid has to be deformed with the local PD magnitude, a number $N_{PD}$ of nodes must be present in $\delta_k(t)$ at every time station. Note that the values of $\mathfrak{N}$, $N_{PD}$, and $k$ can vary from line to line.

Thus, each line suffers a quasi-one-dimensional treatment during each time step of the evolution (see Fig. 2).

1) The velocity of the boundary node $P_1$ of the line is computed and integrated in time (see next section) to yield the displacement $\Delta P_1$ of the boundary due to ablation in the direction normal to the boundary. All other nodes of the line are moved proportionaly.

2) If required, an explicit displacement of the $(N_{PD})$th node of the line is prescribed in the direction of the line, so that its instantaneous position is equal to $\delta_k(t)$ given by Eq. (31) and either Eqs. (27) or (28) ($N_{PD}=2$ in the case of Fig. 2). All other nodes of the line are then assigned a corresponding explicit displacement: dilation for $j<N_{PD}$ or contraction for $j>N_{PD}$.

Steps 1 and 2 are made iteratively until convergence is reached.

Nodal velocities are finally computed and interpolated with the same shape functions as the temperature to build the convective matrix of Eq. (21). Discretization lines transversing the master lines are then deformed sequentially and automatically. The procedure is most often initialized with a uniform grid that is usually too coarse in the vicinity of the ablative boundary. The deformation of the mesh along a line caused by the PD variation (step 2) is stopped when the

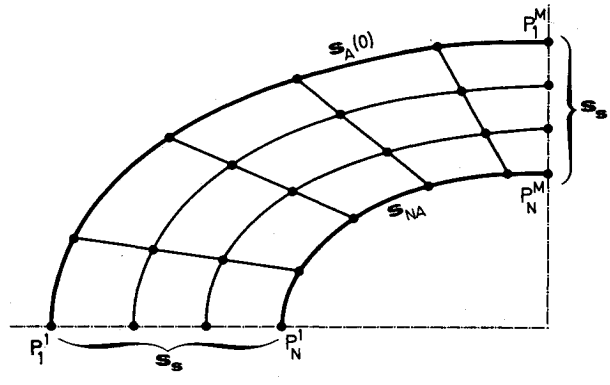


**Fig. 1 Boundaries classification and master lines display.**

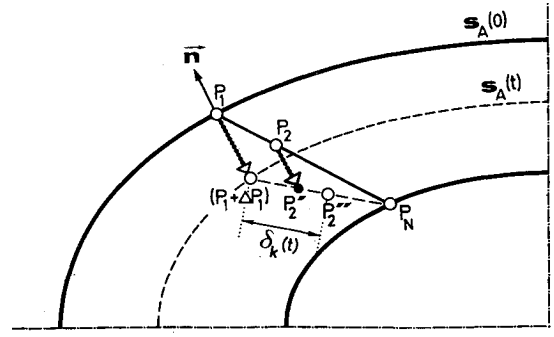


**Fig. 2 Master lines deformation for steep gradient modeling and surface ablation tracking.**

relative positions of the nodes corresponding to the initial mesh are restored.

## Solution of the Spatially Discretized Equations

### Time Integration via Backward One-Step Scheme

Equation (15) is integrated in time using the one-step backward difference scheme,[8]

$$\dot{q}_{n+1} = (q_{n+1} - q_n)/\Delta t, \quad \Delta t = t_{n+1} - t_n \tag{32}$$

where the subscripts denote the corresponding time station. We are then led to the set of nonlinear algebraic equations in terms of $q_{n+1}$

$$(K - K^d + C/\Delta t)_{n+1}\, q_{n+1} = g_{n+1} + g^a_{n+1} + C_{n+1}\, q_n/\Delta t \tag{33}$$

which is to be solved together with the system of equations (23) with the constraints of Eq. (26), all written at $t_{n+1}$.

Once the ablation velocities are known, the same time difference as Eq. (32) is applied for the node movements due to ablation and PD deformation, yielding $s_{n+1}$ and $\delta(t_{n+1})$ through the difference equations

$$\dot{s}_{n+1} = (s_{n+1} - s_n)/\Delta t \tag{34}$$

$$\delta^2(t_{n+1})/\beta_w(t_{n+1}) - \delta^2(t_n)/\beta_w(t_n) = \Delta t\,[1 - \dot{s}_{n+1}\ \delta(t_{n+1})/\beta_w(t_{n+1})] \tag{35}$$

### Iterative Solution Procedure

The nonlinear system of Eqs. (23-33) is solved iteratively using a modified Newton-Raphson method; i.e., starting with predicted values $(q_{n+1})^i$, $(v^f_{n+1})^i$, $(v^c_{n+1})^i$, $(v^m_{n+1})^i$, one searches for corrections to these values by solving the linearized systems

$$(K - K^d + C/\Delta t)^i_{n+1}\, \Delta q_{n+1} = r^i_{n+1} \tag{36a}$$

$$(L^f_{n+1})^i\, \Delta v^f_{n+1} = (r^f_{n+1})^i \tag{36b}$$

$$(H^c_{n+1})^i\, \Delta v^c_{n+1} = (r^c_{n+1})^i \tag{36c}$$

$$(H^m_{n+1})^i\, \Delta v^m_{n+1} = (r^m_{n+1})^i \tag{36d}$$

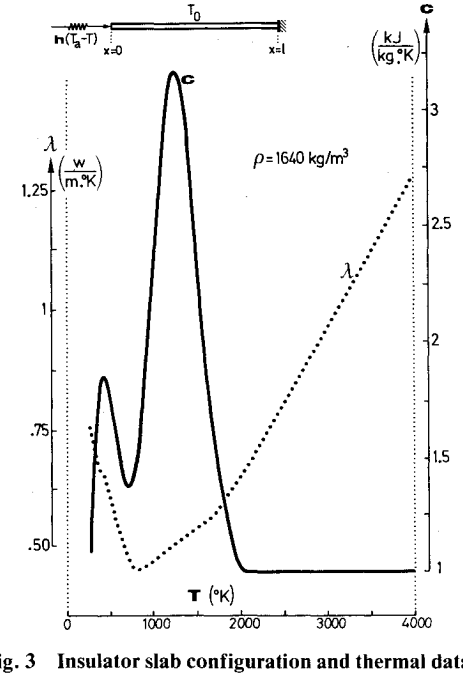


**Fig. 3 Insulator slab configuration and thermal data.**

where the right-hand sides of these equations are the values of the residual vectors of Eqs. (23-33) in terms of the predicted values. Once computed, the corrections are added to these values to yield the $(i+1)$th iterate. The iterative procedure is initialized by taking as the first estimate the values of the variables at time $t_n$ and is stopped when an appropriate relative norm of the residual vectors becomes smaller than the convergence threshold.

Note that Eq. (36b) is subject to the constraints derived from Eq. (26), i.e.,

$$(\Delta v^f_{n+1})_\ell = -(v^f_{n+1})_\ell \text{ if } (\Delta q_{n+1})_\ell < T_f - (q_{n+1})_\ell$$

$$(\Delta v^f_{n+1})_\ell \geq -(v^f_{n+})_\ell \text{ if } (\Delta q_{n+1})_\ell = T_f - (q_{n+1})_\ell \tag{37}$$

where $\ell$ denotes the current component of the surface velocity and temperature vectors and the small $(M \times M)$ systems [Eqs. (36b-36d) are solved by direct inversion (with system matrices in either consistent or lumped form) and include the values $q^{i+1}_{n+1}$ yielded by the global system [Eq. (36a)] at the current iteration. The latter is unsymmetrical due to the presence of the convective matrix and requires a special organization of the block-by-block solution algorithm.

### Constraints for Phase Change Ablation

In case of phase change ablation, the surface temperature may never overcome the corresponding phase change temperature $T_f$. When the latter is reached in the transient response, the boundary temperature remains fixed and the phase change absorbs the additional heat input. Constraints of the type of Eq. (37) are thus added to Eq. (36a)

$$(\Delta q_{n+1})_\ell \leq T_f - (q_{n+1})_\ell \tag{38}$$

with a corresponding positive residual in case of ablation, i.e.,

$$(r_{n+1})_\ell \geq 0 \text{ if } (\Delta q_{n+1})_\ell = T_f - (q_{n+1})_\ell \tag{39}$$

meaning that the fixation at $T_f$ results from a heat input. The problem of Eq. (36a) under the constraints of Eqs. (38) and (39) is then solved at every iteration using a linear equation solver with inequality constraints[9] that has been modified for nonsymmetric systems. The algorithm proceeds by freeing the surface temperature unknowns, initially fixed at $T_f$, in the decreasing order of importance of their associate residual vector component $(r_{n+1})_\ell$, until Eqs. (38) and (39) are satisfied.[10] Therefore it deals only with the $M$ surface unknowns and is very inexpensive to use.

### Space and Time Step Restrictions

In order to insure a unique solution to the above system of equations, we must guarantee the positive definite character of the iteration matrix. The latter reads for a one-dimensional element with linear shape functions, unit cross-sectional area, and length $\ell$,

$$K - K^d + \frac{C}{\Delta t} = \frac{\lambda}{\ell}\begin{bmatrix} 1 & -1 \\ -1 & 1 \end{bmatrix} + \frac{\rho c}{6}\begin{bmatrix} 2u_1 + u_2 & -(2u_1 + u_2) \\ u_1 + 2u_2 & -(u_1 + 2u_2) \end{bmatrix} + \frac{\rho c \ell}{6\Delta t}\begin{bmatrix} 2 & 1 \\ 1 & 2 \end{bmatrix} \tag{40}$$

where $u_1$ and $u_2$ are the nodal velocities due to grid motion. The positive definite character of this system is guaranteed if

$$u_{\max}\Delta t/\ell < \tfrac{1}{2} \tag{41}$$

where $u_{\max}$ is the greatest nodal velocity in modulus

$$u_{\max} = \max(|u_1|, |u_2|) \tag{42}$$

Equation (41), which may be very stringent, can be extended to two-dimensions by taking $u_{max}$ as the greatest nodal velocity component (in modulus) and $\ell$ as the smallest dimension of the element.

#### Convergence Difficulties in Case of Severe Chemical Ablation

$f_c$ [see Eq. (8)] can exhibit very sharp variations with temperature (quasistep functions) and consequently the associate discretized thermal loads also [Eq. (20) or (25b)] since they depend explicitly on that function. This can lead to convergence difficulties or even lack of convergence in the context of the modified Newton-Raphson technique [Eq. (36a)]. To remedy this situation, it has been decided to include in the iteration matrix of Eq. (36a) the Jacobian matrix of these loads with respect to the temperature unknowns, i.e.,

$$J_{in} = \frac{\partial g_i^c}{\partial q_n} = \int_{S_2(t)} \frac{\partial}{\partial T}\{\rho[H_c + \eta(H_a - H)]f_c\}\psi_i\psi_n \mathrm{d}S \tag{43}$$

This yields an iterative procedure where one of the search directions is at least tangent to the thermal load curve, which greatly improves the overall convergence rate. Nevertheless, convergence difficulties can subsist in the case of sharp temperature variations in $f_c$ separating two ranges of constant values, for which the only remedy for convergence is a substantial reduction in the time step.

## Numerical Illustrations

Conventional one- and two-dimensional isoparametric finite elements have been transformed according to the present deforming grid formulation, and special one- and two-dimensional boundary elements have been devised to build the surface ablation systems. They have been inserted in a special-purpose computer program[10] and tested on a variety of model problems. Some of them will be illustrated here.

#### One-Dimensional Phase Change Ablation of an Insulating Material

The thermal characteristics of the material depend on temperature as reported on Fig. 3, where we note very low thermal conductibility values and sharp variations in the heat capacity, yielding highly nonlinear material properties. Phase change ablation occurs at $T_f = 2500$ K with a latent heat $L_f = 4000$ kJ/kg.

A slab of width $\ell = 15 \times 10^{-3}$ m is initially discretized with 15 linear and equally spaced elements. The initial temperature is $T_0 = 300$ K. The face $x = 0$ is attacked by a convective flux with $T_a = 3000$ K and a time- and temperature-dependent exchange coefficient $h$, whose values are obtained from Table 1 via linear interpolations. The face $x = \ell$ is insulated.

The grid is deformed at the same time for ablation and steep gradient modeling purposes with $k = 4$ and $N_{PD} = 14$. The transient response is integrated with $\Delta t = 0.25$ s. The corresponding results for the surface recession and temperature are reported on Fig. 4. They are compared to an existing (finite difference) numerical solution[11] with variable time steps that detects ablation at $t_i = 1.57$ s. The maximum number of iterations per step is five.

The accuracy of our solution has been checked by comparison with coarser discretizations obtained 1) by doubling the time step to $\Delta t = 0.5$ s and 2) by reducing the number of elements in a ratio 2/3 (10 elements with $k = 4$ and $N_{PD} = 8$). Major discrepancies (Fig. 4) are encountered with modification 2, which is not surprising in view of the nonlinear material data. The maximum number of iterations per step were 7 and 20 for runs 1 and 2, respectively.

#### Two-Dimensional Model Phase Change Problem

A model two-dimensional problem is next analyzed; it corresponds to the phase change ablation of one-half of a hollow sphere made of carbon. (See Fig. 5 for the associated thermal data, where we note a conductibility 100 times larger than in the first example.)

The radii of the sphere are $r_i = r_e/5 = 10 \times 10^{-3}$ m. The initial spatial discretization is uniform and limited to one-quarter due to axisymmetrical conditions, with $5 \times 5$ quadrilateral four nodes elements ($\Delta r = 8 \times 10^{-3}$ m, $\Delta\theta = 18$ deg).

The initial temperature is $T_0 = 300$ K and the heat input consists of a convective flux $h(T_a - T)$ at $r = r_e$ with $T_a = 5000$ K and a variable exchange coefficient given in Table 2. The latter depends on temperature and time as in example 1 and also on the azimuthal angle $\theta$ in such a way that a maximum exchange (and ablation) occurs on the symmetry axis. The inner surface is insulated. Ablation occurs at $T_f = 3800$ K with a phase change latent heat $L_f = 10^4$ kJ/kg.

The transient response is integrated using $\Delta t = 1$ s and the ablation results are reported in Figs. 6 and 7, which respectively show the initial and final (deformed) finite element grids and the successive positions of the ablative boundary $s(t)$ with isothermal plots for $t = 5$ s. Note how the phase change propagates with time along the surface due to the spatial variation of the exchange coefficient until covering the whole of it for $t = 4$ s.

Note that surface recession is maximum at the stagnation point for the same reason, while ablation is speeded with time due to the time dependence shown in Table 2. In this example, the grid was deformed only for ablation purposes: the thermal gradients concentrate near the attacked boundary, but are not steep enough to require any specific deformation of the mesh. The maximum number of iterations per step was six for this analysis. A final remark about the lumped or consistent form of the ablation matrices appearing in Eq. (23): it is essential that consistent matrices be used to avoid overestimation of the ablation rates near the symmetry axis.[12]

#### Chemical and Mechanical Ablation of Carbon in Typical Re-entry Configuration

The final example deals with the transient analysis of an axisymmetrical carbon tip under re-entry conditions. The structure is represented in Fig. 8 with the initial finite element grid: it is made of carbon with the same thermal data as in example 2. Ablation takes place at the outer surface of the spherical part under the combined mechanical-chemical explicit models. The mechanical ablation rate is defined as

$$\dot{s}_m = a e^{-T_E/T}(\tau + b p_e)$$

where $a = 10^{-9}$ m/s Pa, $b = 1$, and $T_E = 300$ K. The detailed time dependencies for $\tau$ and $p_e$ cannot be given here. In any case, the former ablation rate is a function with very mild variations and is quite negligible with respect to the chemical ablation. The latter is defined by the strongly temperature-dependent ablation rate function reported in Table 3.

**Table 1 Variable convective exchange coefficient $h$, (kW/m$^2$ · K)**

| $T$, K | 200 | 2000 | 3000 |
|---|---|---|---|
| $t = 0$ s | 0 | 0 | 0 |
| $t = 10$ s | 8.93 | 25 | 25 |

**Table 2 Convective exchange coefficient for the sphere, (kW/m$^2$ · K) [$h(T,t,\theta) = h_1(\theta)h_2(T,t)$]**

| $\theta$, deg | 0-18 | 18-36 | 36-54 | 54-72 | 72-90 |
|---|---|---|---|---|---|
| $h_1$ | 1.0 | 1.5 | 2.0 | 2.5 | 3.0 |
| | $T$, K | 200 | 1000 | 3000 | 5000 |
| $h_2$ | $t = 0$ s | 0 | 0 | 0 | 0 |
| | $t = 10$ s | 10.83 | 25 | 50 | 50 |

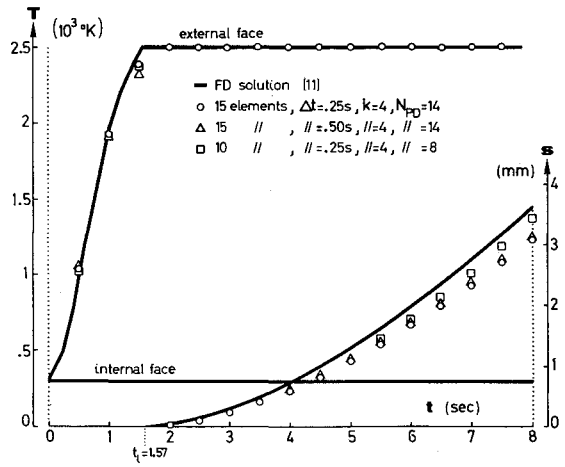


Fig. 4 Insulator slab surface ablation and temperature.

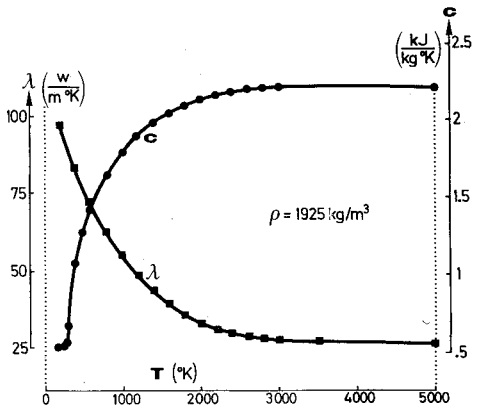


Fig. 5 Carbon thermal data.

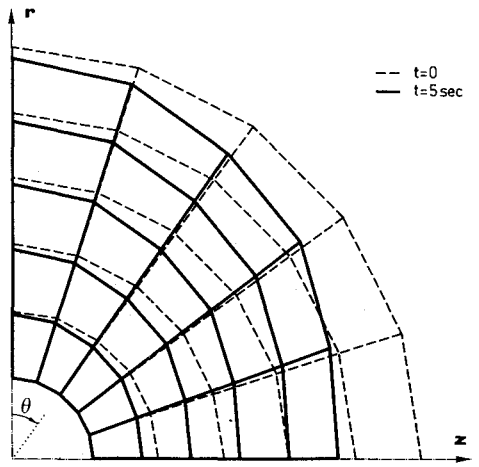


Fig. 6 Carbon sphere, initial and final (deformed) grid.

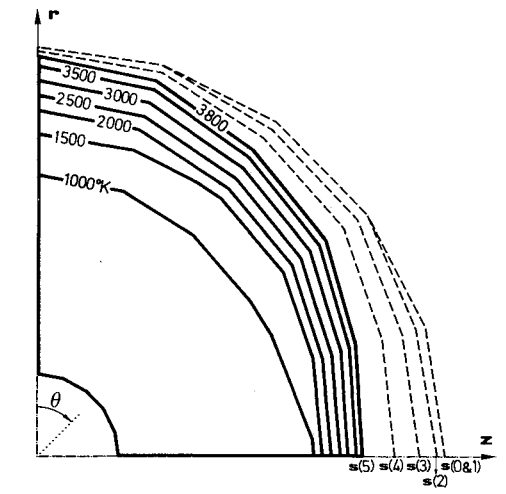


Fig. 7 Carbon sphere, ablative boundary position $s(t)$ and isothermal curves for $t = 5$ s.

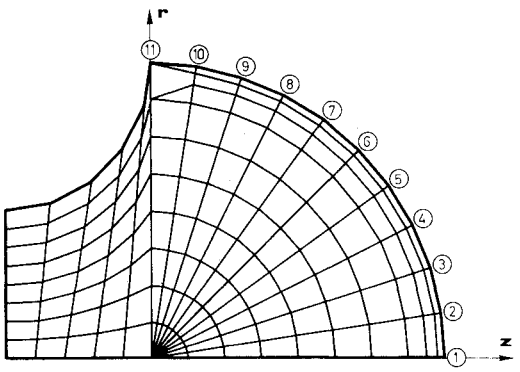


Fig. 8 Initial finite element grid for re-entry tip with identification of ablative boundary nodes.

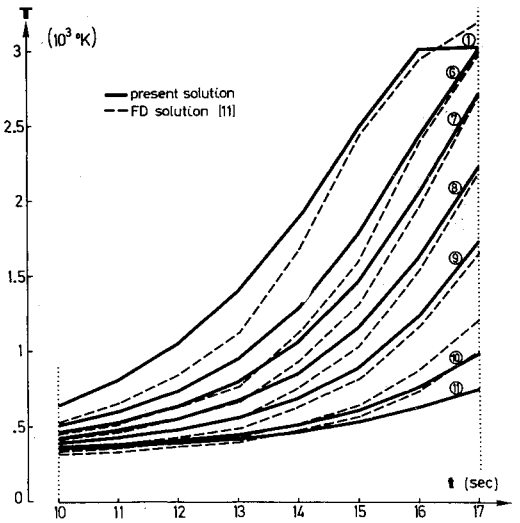


Fig. 9 Re-entry tip, ablative boundary nodes transient temperatures.

Heating along the spherical surface is by convection in enthalpy form with given time variations for $\alpha$ and $H_a$ and $H$ is computed from the boundary temperature via a Mollier catalog. Radiative heating is also considered with a fixed-source temperature $T_r = 300$ K and $\epsilon = 0.9$. The remainder of the outer surface is insulated. The initial temperature is $T_0 = 300$ K and $\eta = 0.5$.

The spatial discretization is based on 110 quadrilateral elements plus 10 triangular and 10 ablation boundary elements, all with linear shape functions. The total number of unknowns is thus 134. The grid is deformed for ablation purposes only and the 11 master lines linking the nodes of the ablative boundary to the center of the sphere are clearly shown in Fig. 8.

The transient temperatures of the 11 surface nodes are shown in Fig. 9 in the range of 0-17 s. Time steps elected for the response integration are 12 times $\Delta t = 1$ s, 7 times $\Delta t = 0.5$ s, and 15 times $\Delta t = 0.1$ s. The substantial reduction of $\Delta t$ in the range of 15.5-17 s is due to steep variations of the thermal loads corresponding to chemical ablation when the surface temperature reaches 3010-3090 K (see Table 3). Below these temperatures, ablation is very mild, which is confirmed by

**Table 3 Nondimensional chemical ablation rate function**

| $T$, K | 300 | 3000 | 3005 | 3010 | 3090 | 3095 | 3100 | 5000 |
|---|---|---|---|---|---|---|---|---|
| $\rho \dot{s}_c/\alpha$ | 0.00 | 0.00 | 0.01 | 0.10 | 0.90 | 0.99 | 1.00 | 1.00 |

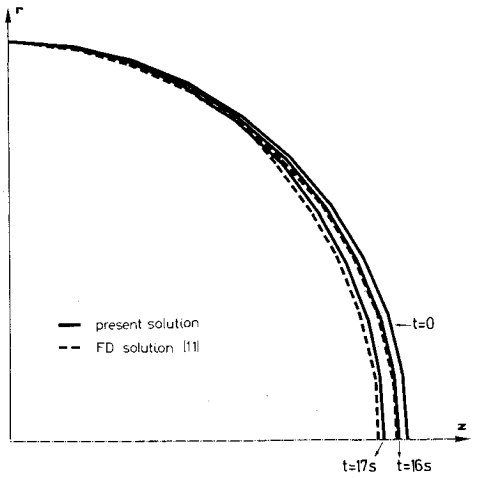


**Fig. 10 Re-entry tip, ablative boundary positions $s(t)$.**

Fig. 10 where the surface recession is plotted for $t = 16$ and 17 s with respect to the initial position. Maximum ablation occurs at the stagnation point (on the axis of symmetry) and consistent ablation matrices had to be used as in example 2. The present results were obtained with a maximum of four iterations per time step and are in good agreement with those obtained via a finite difference code.[11] Convective heat inputs are managed in different ways in the two programs, which can explain the discrepancies between the two solutions (lower ablation rates in the present solution).

## Conclusions and Future Work

Deforming-grid techniques have received a sound formulation in the context of the finite element method. They imply the construction of a special convective matrix at the element level and the definition of a moving-grid strategy. The ability of these techniques to treat surface ablation problems in two-dimensional situations has been demonstrated on model and practical problems.

Further developments will deal with problems where preliminary pyrolysis of the material occurs. Hence, an internal chemical reaction balance has to be coupled with the heat-transfer equations, and the latter have to take into account the heat transported by the gaseous products of that reaction. These intented developments will generalize ideal one-dimensional models based on the hypothesis of a pyrolysis surface.[1]

## References

[1] Hogge, M. and Gerrekens, P., "One-Dimensional Finite Element Analysis of Thermal Ablation with Pyrolysis," *Computer Methods in Applied Mechanics and Engineering*, Vol. 33, 1982, pp. 609-634.

[2] Meyer, G. H., "The Numerical Solution of Multi-dimensional Stefan Problem—A Survey," *Moving Boundary Problems*, edited by D. G. Wilson, A. D. Solomon, and P. T. Boggs, Academic Press, New York, 1978, pp. 73-89.

[3] Chin, J. H., "Charring Ablation by Finite Elements," *Numerical Methods in Thermal Problems II*, edited by R. W. Lewis, K. Morgan, and B. A. Schrefler, Pineridge Press, Swansea, Wales, 1982, pp. 218-229.

[4] Hogge, M. and Gerrekens, P., "Steep Gradient Modelling in Diffusion Problems," *Numerical Methods in Heat Transfer II*, edited by R. W. Lewis, K. Morgan, and B. A. Schrefler, John Wiley & Sons, New York, 1983, pp. 73-97.

[5] Lynch, D. R. and O'Neill, K., "Continuously Deforming Finite Elements for the Solution of Parabolic Problems, with and without Phase Change," *International Journal for Numerical Methods in Engineering*, Vol. 17, 1981, pp. 81-96.

[6] Biot, M. A., *Variational Pinciples in Heat Transfer*, Oxford University Press, London, 1970.

[7] Zien, T. F., "Approximate Calculation of Transient Heat Conduction," *AIAA Journal*, Vol. 14, 1976, pp. 404-406.

[8] Hughes, T.J.R., "Unconditionally Stable Algorithms for Nonlinear Heat Conduction," *Computer Method in Applied Mechanics and Engineering*, Vol. 10, 1977, pp. 135-139.

[9] Fleury, C., LTAS, University of Liège, Belgium, private communication, 1982.

[10] Gerrekens, P. and Hogge, M., "AMARYLLIS—Module de réponse thermique avec ablation et maillage variable," University of Liège, Belgium, LTAS Rept. SF-106, 1982.

[11] Fusade, L. and Rivas, A., "A Computer Program for Transient and Axisymmetric Ablation, Conduction and Radiation," *Numerical Methods in Thermal Problems I*, edited by R. W. Lewis and K. Morgan, Pineridge Press, Swansea, Wales, 1979, pp. 1004-1013.

[12] Hogge, M. and Gerrekens, P., "Two-Dimensional Deforming Finite Element Methods for Surface Ablation," AIAA Paper 83-1555, 1983.